ARMY RESEARCH LABORATORY

Fracture of Grooved Kinetic Energy Rods Subject to Oblique Impact

by Robert L. Anderson

ARL-TR-3923 **September 2006**

NOTICES

Disclaimers

Army Research Laboratory
Aberdeen Proving Ground, MD 21005-5066

ARL-TR-3923 **September 2006**

Fracture of Grooved Kinetic Energy Rods Subject to Oblique Impact

Robert L. Anderson
Weapons and Materials Research Directorate, ARL

REPORT DOCUMENTATION PAGE	*Form Approved* *OMB No. 0704-0188*

1. REPORT DATE *(DD-MM-YYYY)* September 2006	**2. REPORT TYPE** Final	**3. DATES COVERED (From - To)** December 2004–June 2006

4. TITLE AND SUBTITLE
Fracture of Grooved Kinetic Energy Rods Subject to Oblique Impact

5a. CONTRACT NUMBER

5b. GRANT NUMBER

5c. PROGRAM ELEMENT NUMBER

6. AUTHOR(S)
Robert L. Anderson

5d. PROJECT NUMBER
62168AH80

5e. TASK NUMBER

5f. WORK UNIT NUMBER

7. PERFORMING ORGANIZATION NAME(S) AND ADDRESS(ES)
U.S. Army Research Laboratory
ATTN: AMSRD-ARL-WM-TC
Aberdeen Proving Ground, MD 21005-5066

8. PERFORMING ORGANIZATION REPORT NUMBER
ARL-TR-3923

9. SPONSORING/MONITORING AGENCY NAME(S) AND ADDRESS(ES)

10. SPONSOR/MONITOR'S ACRONYM(S)

11. SPONSOR/MONITOR'S REPORT NUMBER(S)

12. DISTRIBUTION/AVAILABILITY STATEMENT
Approved for public release; distribution is unlimited.

13. SUPPLEMENTARY NOTES

14. ABSTRACT

Kinetic energy penetrators often possess buttress grooves that are used to aid in the launching process. The shock physics code CTH has been used to analyze the effect that these grooves have on tungsten heavy alloy rods during oblique impacts that create asymmetric loading conditions. To examine this behavior, simulations were run in which grooved rods underwent 60° oblique impacts with finite thickness rolled homogeneous armor steel plates at 1300 m/s. Previous experimental work done by Raftenberg and Bjerke has shown that buttress grooves make the rods more susceptible to fracture, and it has been shown that CTH can predict the occurrence of fracture due to stress concentrations in bending loading when the simulation is run using reverse ballistics. The use of reverse ballistics has been shown to decrease the loss of groove definition.

15. SUBJECT TERMS
oblique impact, kinetic energy rod, bending, fracture, buttress groove

16. SECURITY CLASSIFICATION OF:			**17. LIMITATION OF ABSTRACT**	**18. NUMBER OF PAGES**	**19a. NAME OF RESPONSIBLE PERSON** Robert L. Anderson
a. REPORT UNCLASSIFIED	**b. ABSTRACT** UNCLASSIFIED	**c. THIS PAGE** UNCLASSIFIED	UL	26	**19b. TELEPHONE NUMBER** (*Include area code*) 410-278-6558

Contents

List of Figures

Acknowledgments

The author would like to thank Todd Bjerke for his continued correspondence with regards to his experimental work. Thank you to Kent Kimsey for his technical review. Also, thank you to Steve Schraml and Kent Kimsey for their helpful suggestions with regards to the simulations. The simulations contained within this report were run using a U.S. Army Research Laboratory (ARL) Major Shared Research Center Linux cluster. Visualization of the scientific data was made possible through the use of tools developed by the ARL Scientific Visualization team.

INTENTIONALLY LEFT BLANK.

1. Introduction

Kinetic-energy (KE) penetrators are often used in military anti-armor applications. These penetrators can have a tendency to fracture during oblique penetration, thereby reducing the rod's ability to penetrate subsequent regions of the target. Under this premise, the military is interested in developing fracture resistant penetrator designs to better resist failure due to the lateral loading applied by oblique impact.

In order to aid in the launching procedure, KE penetrators often have a series of buttress grooves covering some portion of the rod length. While exploring possibilities for fracture resistant penetrator design, a combined experimental and computational investigation by Raftenberg and Bjerke (*1*) focused on the effect that the buttress grooves have on rod breakup. The experiments involved firing ARL6A-T and ARL7-T rods composed of 93.1W-4.7Ni-2.2Co tungsten heavy alloy (WHA) at nominally 1300 m/s. The targets used were 9.5-mm rolled homogeneous armor (RHA) plates at 60° obliquity. Under these shot conditions, it was observed that rod breakup tended to occur. Also, a third set of firings involved ARL7-NT rods that contained no buttress grooves and were launched by means of a pusher plate method. The ARL7-NT rod experiments yielded varied results, leading to the conclusion that the grooves make the rods more susceptible to fracture.

Observations from a similar study (*2*) showed that rod fracture tended not to occur for shots against relatively thinner targets. Experimentally, it was determined using the ARL7-T rod that the critical threshold for which fracture would occur is

$$\frac{t}{d} \cong 1 . \tag{1}$$

In equation 1, t is the plate thickness, and d is the critical rod diameter. The critical rod diameter is defined as the minimum rod diameter at the groove root.

The scope of this report is to examine the capability of CTH, an Eulerian shock physics code, to predict rod breakup under simulated experimental conditions. Computational studies were performed using the ARL6A-T rod and an ungrooved version analogous to the ARL7-NT rod to examine the code's ability to predict fracture and to verify and characterize the fracture mechanisms that have been seen experimentally. Simulations were run using forward ballistics (rod in motion) and reverse ballistics (target in motion) simulations. The reverse ballistics simulations yield better results. Also, a computational study was done to examine the plate thickness effects of equation 1 using the ARL6A-T rod.

2. Computational Method

Using a commercially available solid modeling software package, a model of the ARL6A-T rod was created from the drawing shown in figure 1. Target plates of various thicknesses were also modeled at their proper obliquity of 60°. The solid model of the projectile and target were then sectioned along a symmetry plane containing the rod axis and plate normal vector to reduce the computational cost of the three-dimensional (3-D) simulation. The next step involved using the Cubit finite-element meshing code to mesh the target and rod volumes with a hexahedron scheme (*3*). Once in this format, CTH possesses a material insertion capability that allows the hexahedral elements to be read directly into a 3-D Eulerian mesh as cell volume fractions. This method was used to create target and rod geometries that were as close as possible to the geometries that were tested experimentally. The impact velocity for all simulations was 1300 m/s. A detailed sketch of the initial impact conditions can be seen in figure 2.

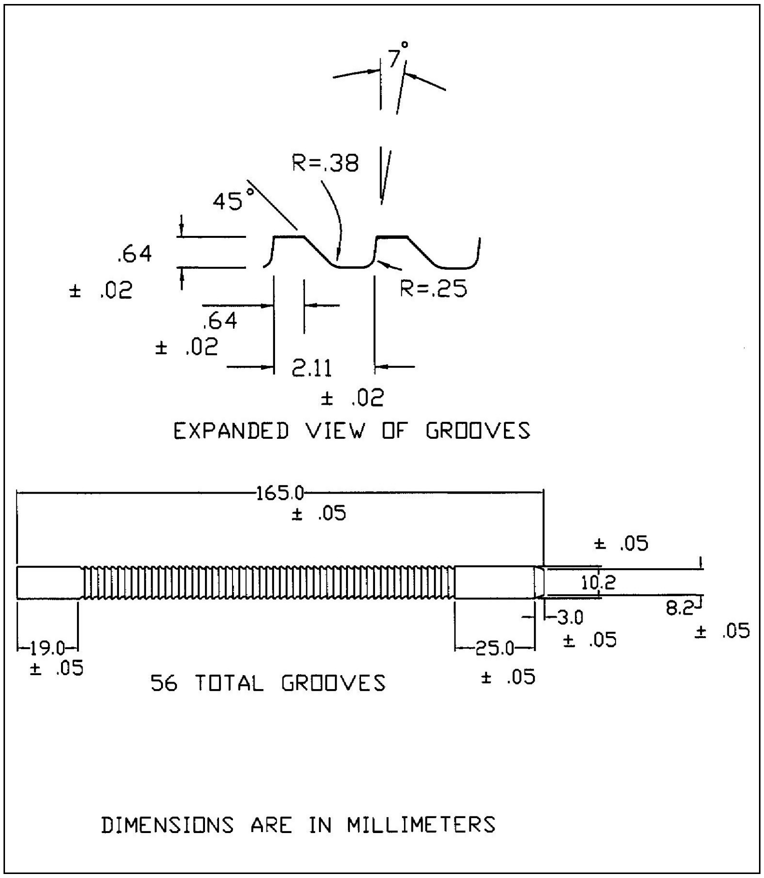

Figure 1. ARL6A-T penetrator geometry (*1*).

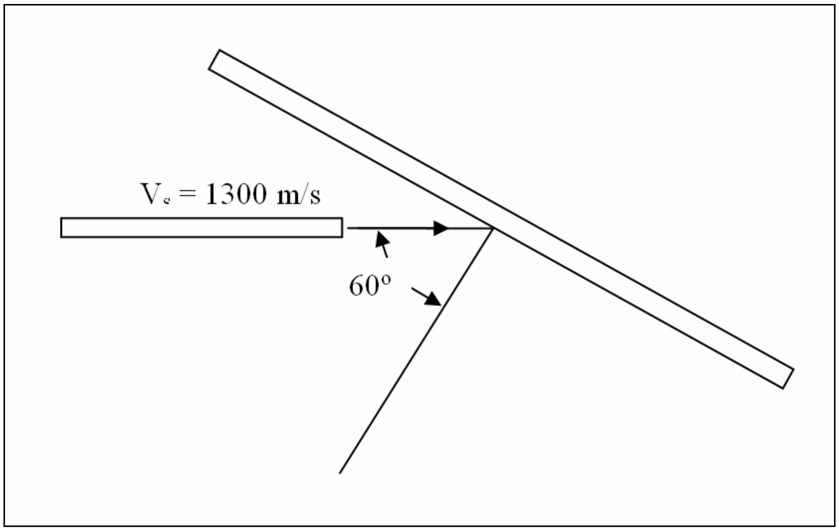

Figure 2. Sketch of impact conditions.

CTH is an Eulerian finite volume shock physics code that provides numerical solutions at finite intervals, or time steps, by using a two-part process involving a Lagrangian step followed by a re-map step. During the Lagrangian step, explicit finite volume equations are solved. For the second-order-accurate re-map step, an operator splitting technique is used to reduce multi-dimensional equations to sets of one-dimensional equations. CTH effectively handles problems involving explosive detonation, shock wave propagation, and elastic-plastic material behavior at high rates of deformation with multiple materials present (*4*). The simulations in this study were run using CTH version 7.0.

The 3-D rectangular Eulerian mesh employed cubic computational cells in the region containing the rod and centered along its trajectory path (*x*-axis) with a uniform cell size of 0.025 cm per side. This size was selected to try to maintain maximum fidelity of the buttress groove geometry during material advection. The mesh was then coarsened in the directions normal to the shot line (*y*- and *z*-directions) with an expansion ratio of 5%. A reflecting boundary condition was prescribed to the mesh at the symmetry plane.

The rod and target plate were both modeled using the Mie-Gruneisen analytical equation of state (EOS). The EOS properties used for the rod were CTH library values for tungsten, except that the density was set to 17.65 g/cm^3. The target plate properties were the standard library values for iron. The rod and target were both modeled using Johnson-Cook constitutive strength and Johnson-Cook cumulative damage models for their respective materials. The rod was modeled using standard CTH library values for tungsten, and the plates were modeled using standard 2IN_RHA values with *aj0* parameter scaling consistent with Meyer and Kleponis (*5*). The Johnson-Cook damage model specifies that for any material with a scalar damage value of unity, failure will occur.

The CTH threshold fracture model was also used for the rod and target. The *stress* keyword was used to indicate that fracture should occur for any material in a cell with a minimum principal stress that is less than the dynamic tensile strength (convention exists that tensile strength values are negative) for that material. When the minimum principal stress exceeds the specified tensile strength for a material, void will be inserted in that cell to prevent stress states from reaching tensile values less than the dynamic tensile strength, thereby creating a fracture surface (*6*). Dynamic tensile strengths were set at –6.89E9 dynes/cm^2 and –2.5E10 dynes/cm^2 for the tungsten rod and RHA target, respectively.

---

3. Effects of Forward Ballistics vs. Reverse Ballistics

The first simulation that was performed was a forward ballistics simulation of the ARL6A-T rod vs. 9.5-mm RHA plate, in which the target was initially stationary and the rod was in motion. Experimentally, it was found that the rod would fracture for these impact conditions, and in five out of five similar tests, a large nose fragment would separate from the larger portion of the rod (*1*).

The simulation results for these conditions can be seen in figure 3a. The rod does not fracture, but a large zone of damage can be seen in figure 3b, which is a close-up view of the nose region.

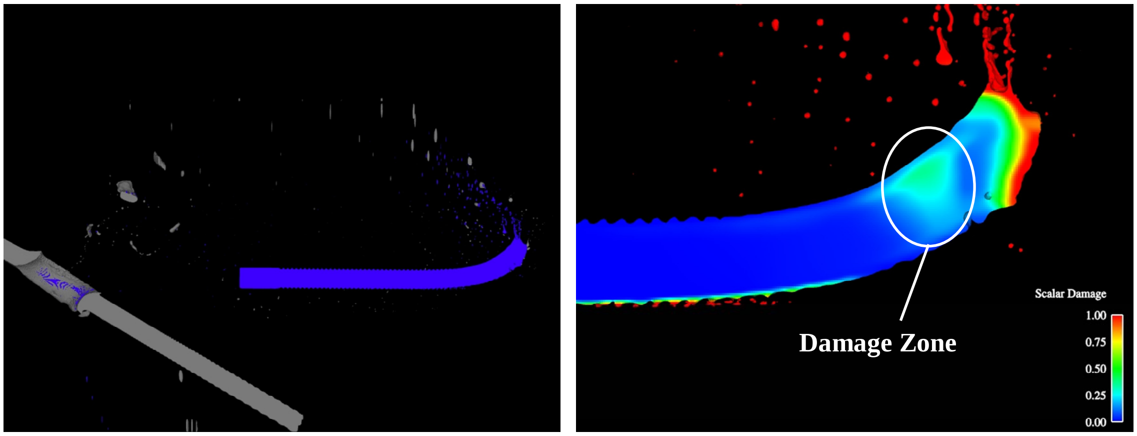

(a) **(b)**

Figure 3. Forward ballistics simulation of ARL6A-T vs. 9.5-mm RHA plate (t = 220 μs): (a) post-impact rod geometry and (b) scalar damage contours.

While the rod does not fracture, the fact that a localized damage zone appears is of interest. This indicates that the rod undergoes higher levels of stress in this zone. Using the results from the forward ballistics simulation, it was hypothesized that if the simulation were run with reverse ballistics (i.e., the rod being stationary and the plate in motion) that this would minimize material advection errors at the buttress grooves and capture stress concentrations in the groove roots. After running the simulation in reverse ballistics, it was observed that the rod could, in fact, be shown to fracture computationally. Figure 4a shows the result of the reverse ballistics simulation. Figure 4b is the reverse-ballistics analog of figure 3b, and it can be seen that along the fracture surface, the scalar damage magnitude is very close to zero, indicating that the rod does not fail by means of the Johnson-Cook damage model.

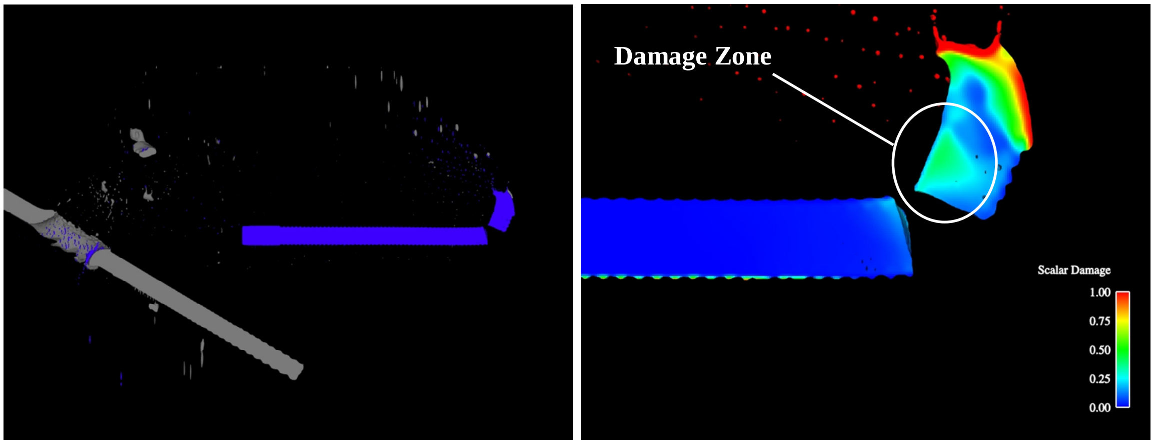

(a) **(b)**

Figure 4. Reverse ballistics simulation of ARL6A-T vs. 9.5-mm RHA plate (t = 220 μs): (a) post-impact rod geometry and (b) scalar damage contours.

The images in figure 5 show an experimental radiograph that corresponds to impact conditions that are consistent with the simulation. It can be seen through direct comparison of figures 4 and 5 that the results are qualitatively consistent from the simulation to the experiment.

As previously stated, the Johnson-Cook cumulative damage model is not the source of the material fracture. The only other failure model that was incorporated was the minimum principal stress criterion used in the CTH threshold fracture model. The plots in figures 6 and 7 represent the extreme minimum principal stress encountered by each cell up to the point in time at which the image was created. The reader should be aware that the stress values shown in figures 6 and 7 do not necessarily correspond to the stress state at a given instant in time. Because the plot represents the extreme value of stress seen by a cell over an entire elapsed time interval, the stress values in the plot will remain constant even after stresses have relaxed back to zero. Figure 6 shows how the CTH shock physics code captures stress concentrations emanating from the groove roots.

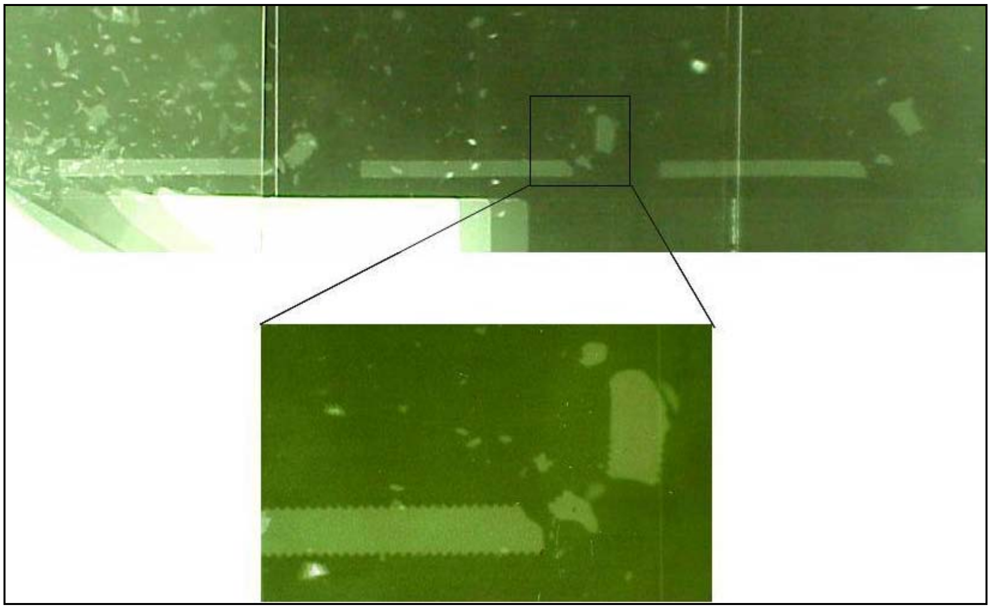

Figure 5. Post-perforation radiograph of ARL6A-T (*1*).

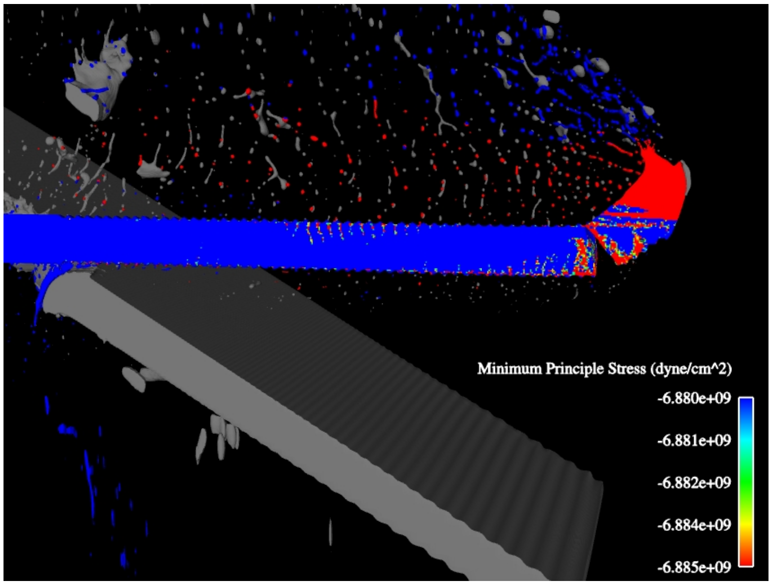

Figure 6. Rod minimum principle stress extrema (t = 145 μs).

In figure 7, the initiation of the crack can be seen, and it is obvious from the stress values indicated that the fracture surface was spawned as a result of void insertion due to material failure as defined by the principle stress-based threshold fracture model.

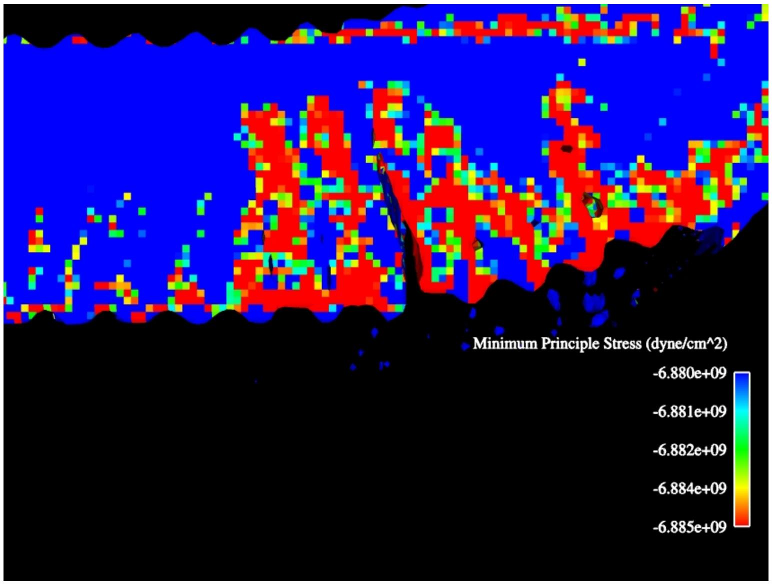

Figure 7. Close-up image of minimum principle stress (t = 95 μs).

One item of interest is the point in time that the lateral loading is applied that causes the fracture to occur. Figure 8 shows that as the rod exits the plate for the 16.1-mm plate, it reaches a state where the rod erosion rate slows and the rod begins to pass through the exit crater.

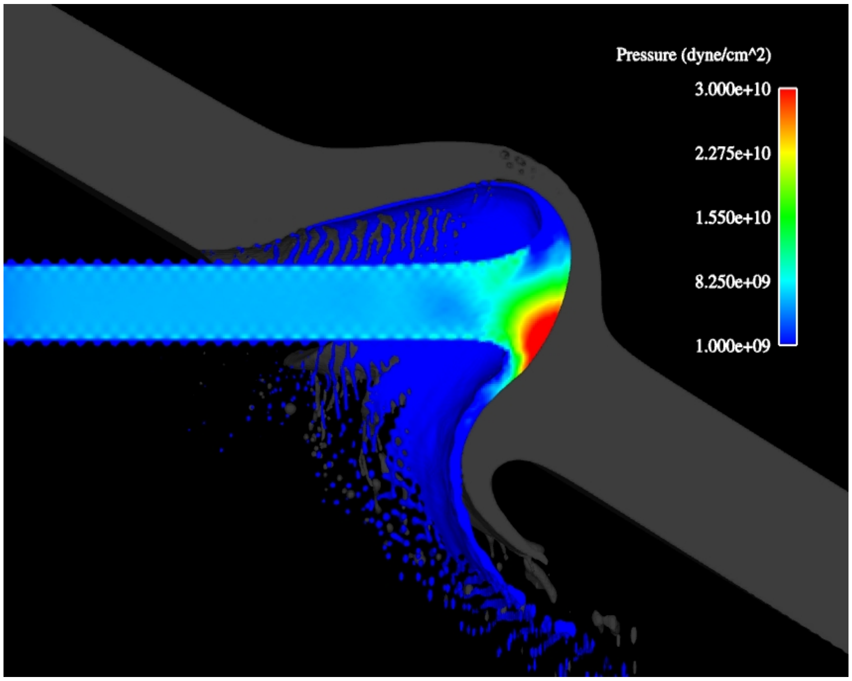

Figure 8. Rod interaction with 16.1-mm RHA plate.

The rounded shape of the exit crater applies a normal force with components that are both upward and rearward. This creates asymmetric loading on the nose. This loading provides the bending force required to break off the tip of the rod near the beginning of the grooved region. Raftenberg and Bjerke (*1*) showed that the buttress grooves cause the rod to be more prone to fracture under bending loads, and the simulation shows the asymmetric (i.e., bending) loading on the rod as it exits the plate.

4. Effect of Grooves — Smooth Rod Shot

In order to verify that the buttress grooves create stress concentrations in the rod, a simulation was performed in which a smooth rod was fired against a 9.5-mm RHA plate at 60° obliquity and a striking velocity of 1300 m/s. The diameter used to construct the smooth rod is the critical diameter of the grooved rod with respect to bending, which is the minimum diameter at the groove roots. To maintain consistency, this simulation was done using reverse ballistics.

For the described conditions, it can be seen in figure 9 that the rod fractures numerically. Consistent with experiments by Raftenberg and Bjerke (*1*) involving the ARL7-NT rod, the fracture surface geometry is quite different from the fracture surface as seen when firing the grooved rod against the same target plate (see figure 4). Experimentally, the grooved rod fracture surface geometries consisted of a structured S-shape, whereas the fracture surface geometries of the smooth rods exhibited more randomness. Similarly, the numerical grooved rod fracture surface shown in figure 4 and the numerical smooth rod fracture surface shown in figure 9 follow the same trends as seen experimentally.

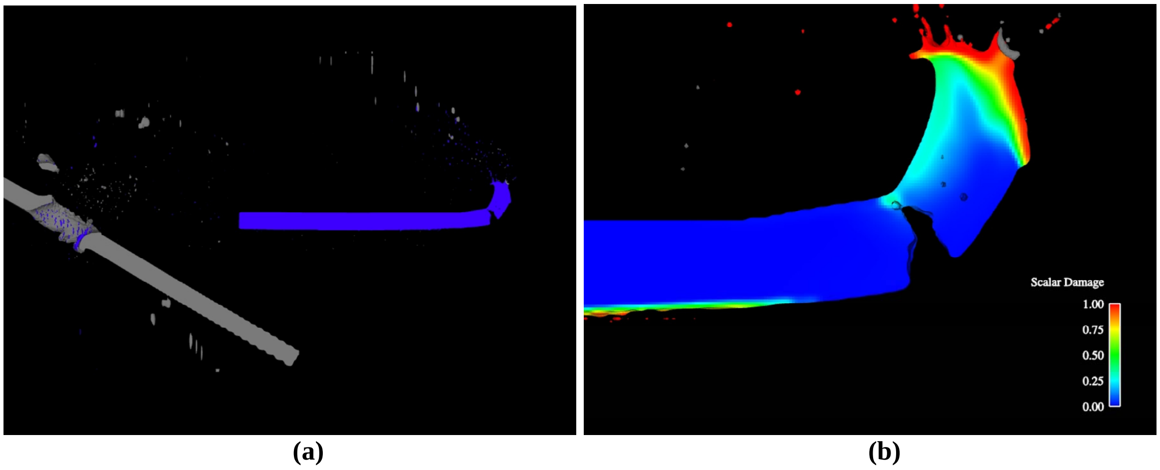

(a) **(b)**

Figure 9. Reverse ballistics simulation of smooth rod vs. 9.5-mm RHA plate (t = 220 μs): (a) post-impact rod geometry and (b) scalar damage contours.

The difference in numerical fracture surface geometry can be attributed to the stress concentration effects of the buttress grooves. The shape of the fracture surface in figure 9 is indicative of a stress pattern that is not as well defined as the sharp concentrations seen in figures 6 and 7. It appears in figure 9 that the fracture initiates at the lower surface of the rod. The tip of the crack then acts as a stress raiser that provides the driving force necessary to propagate the fracture of the rod, and as it does so, it traverses a somewhat random path. In figure 9b, a small void can be seen at the tip of the crack. This void is due to the CTH threshold fracture model and has been inserted per criteria outlined in section 2. Conversely, the fracture of the grooved rod is due to the sudden onset of sharp stress gradients as seen in figures 6 and 7 that are developed due to the geometric discontinuities at the grooves.

In experiments performed by Raftenberg and Bjerke (*1*), fracture occurred with less frequency and with great variation in the crack location for the cases in which fracture did occur. Raftenberg and Bjerke cited material flaws and machining imprecision as the cause of the randomness in the fracture surface geometry and its location on the rod. The numerical simulations support this case. If simulations were run using a stochastic constitutive model for the rod material, the fracture location in the numerical runs may be subject to the same random behavior.

5. Plate Thickness Effects

Experimental data by Raftenberg and Bjerke (*2*) regarding plate thickness effects have shown that for the ARL7-T rod fired at conditions consistent with figure 2, failure would occur for a target thickness to critical rod diameter ratio (see equation 1) of ~1. The experimental data show that for a t/d ratio of 0.4, fracture does not occur, but does occur for t/d = 0.9 and t/d = 1.8. Using experimental data as guidance, simulations were run using the ARL6A-T rod with target thicknesses of 3.6, 9.5, and 16.1 mm. This provided t/d ratios similar to the experiments. The results of these simulations are shown in figure 10. For the two images in which fracture occurs, the rod appears to separate in the same location—six grooves aft of the transition between the grooved and ungrooved sections of the penetrator. The fracture location is consistent with what is seen in figure 5. In figure 5, the crack responsible for the detachment of the second fragment initiates approximately five grooves from the nose of the penetrator. The fragment in figure 10c is smaller than that in figure 10b due to the additional erosion that occurred during the penetration of the thicker target.

The images in figure 11 show the scalar damage plots of the rods in the plate thickness effect study. In the images that involve fracture, it is evident that for neither case did the fracture occur based on the scalar value of the Johnson-Cook damage model. Note that as the plate thickness increases, the scalar damage values indicate an increase in the severity of the loading on the rod.

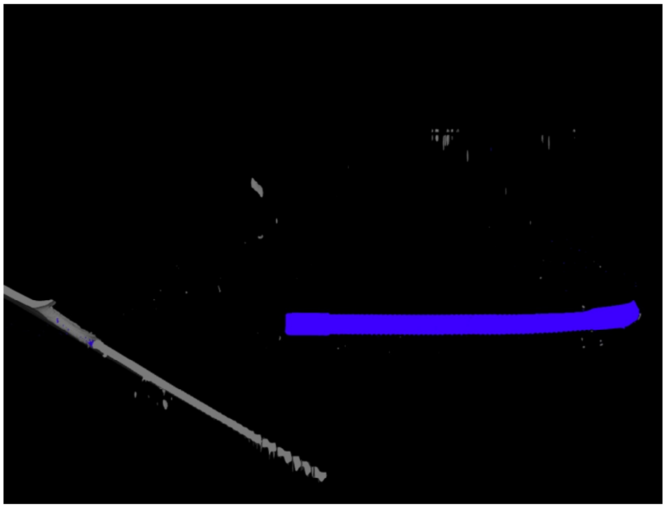

(a) (t = 220 ms)

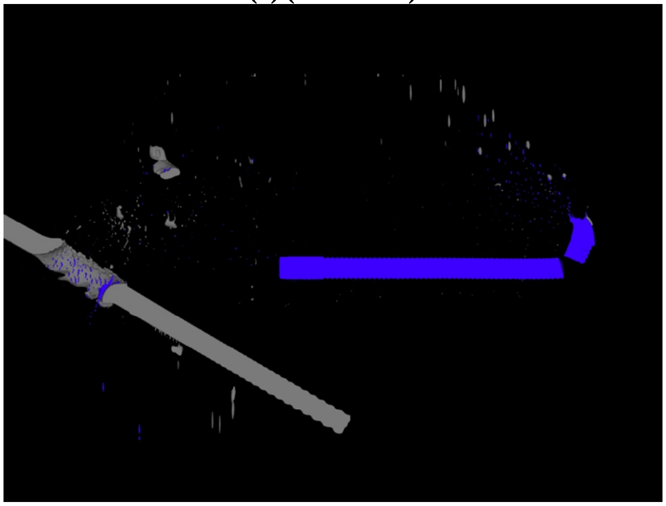

(b) (t = 220 ms)

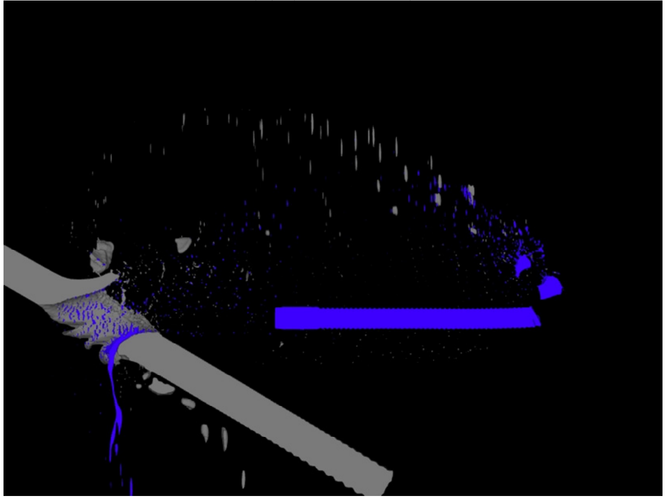

(c) (t = 220 ms)

Figure 10. Computational results of critical t/d ratio study: (a) t/d~0.4, (b) t/d~0.9, and (c) t/d~1.8.

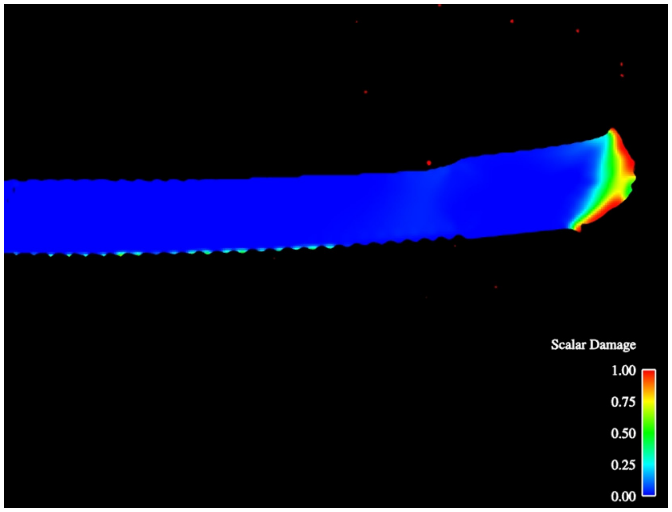

(a) (t = 220 ms)

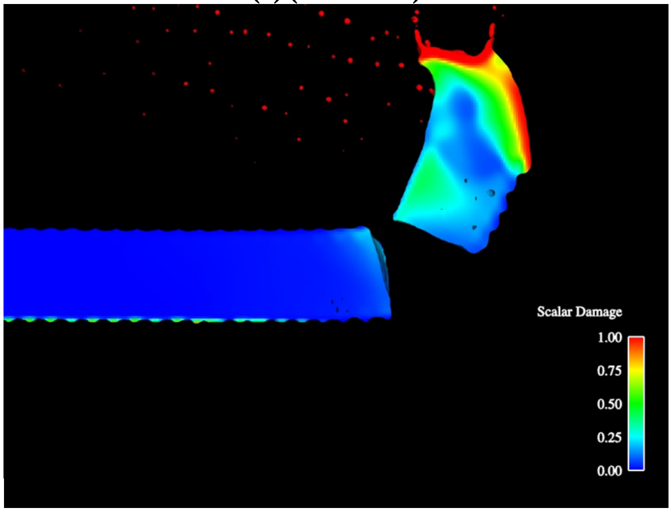

(b) (t = 220 ms)

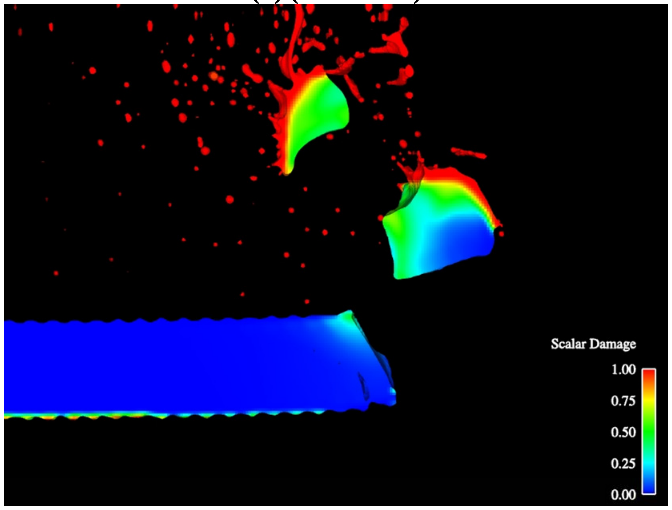

(c) (t = 220 ms)

Figure 11. Scalar damage contours for critical t/d ratio study: (a) t/d~0.4, (b) t/d~0.9, and (c) t/d~1.8.

6. Material Advection Sensitivity Study

The reason the penetrator fails in reverse ballistics and not in forward ballistics can be attributed to loss of geometric sharpness as the penetrator material fluxes through the grid. The CTH interface tracking scheme that was used was the second-order-accurate Sandia Modified Youngs' Reconstruction Algorithm (SMYRA), which is the recommended option when running 3-D problems (*7*). To examine the interface tracking ability of CTH SMYRA with the given resolution, a simulation was run for 330 μs without a target present, and buttress groove-profile images were generated at the initial and ending times. Figure 12 shows a comparison of the groove geometry for the (a) original finite-element model, (b) CTH model at time = 0 μs, and (c) CTH model at time = 330 μs. It is evident from comparison of (b) and (c) that as the penetrator material fluxes through the grid, the geometric sharpness of the grooves is lost, and thereby lessens the stress concentration factor.

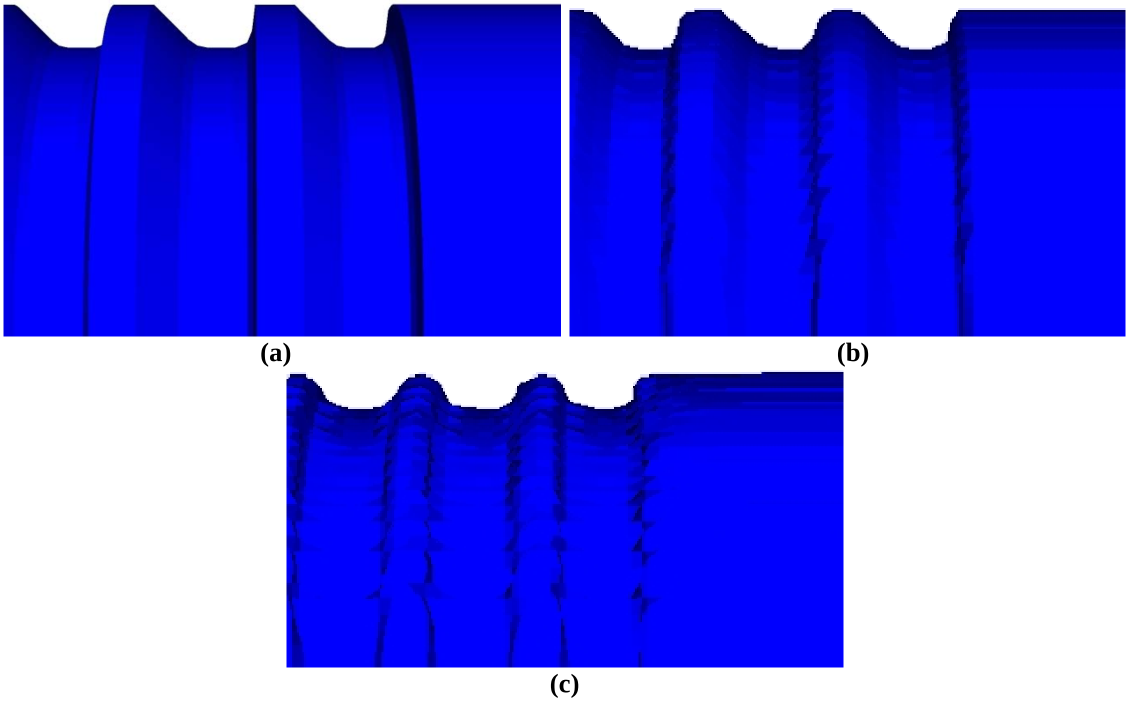
(a)
(b)
(c)

Figure 12. Comparison of buttress groove resolution for (a) finite-element model, (b) CTH representation at t = 0, and (c) CTH representation after 43 cm of advection.

A comparison between figure 12b and figure 12c shows that, for the cell size used in the simulations run for this study, the grooves transform from their original, structured geometry to a rounded, sinusoidal shape. The more rounded shape would not lend itself to as great of a stress concentration factor as the original solid model configuration. Clearly, the sensitivity to material advection on stress concentrations is paramount in accurately predicting fracture at groove roots (see figure 3b and figure 4b). This effect could be lessened by increasing the Eulerian mesh resolution, which would increase the computational requirement.

7. Summary

Overall, it has been shown that the CTH shock physics code can be shown to predict fracture of buttress-grooved long-rod penetrators. The fracture surface initiates because the minimum principal stress in the rod is less than the dynamic tensile strength of the material (convention exists that tensile strength values are negative in CTH). The tensile strength value is exceeded due to stress concentrations at the traction grooves when the rod experiences a bending load as it passes through the oblique target. The effects of the grooves can be contrasted with the results of the smooth rod simulation, which has a much different fracture surface geometry.

Two different versions of the grooved rod simulation were run. In the first simulation, the rod was fluxed through the Eulerian mesh, and the target was stationary. In the second simulation, the reverse was true. The fracture prediction abilities of the code seem to be enhanced when the item of greatest geometric detail—the rod—remains stationary and the target is fluxed through the grid instead. It is shown that this is due to loss of geometric fidelity caused by the advection scheme.

It was shown in experimental data by Bjerke (*2*) that there exists a point when the t/d ratio exceeds some critical value, fracture of the rod will occur. Experimentally, the transition from no fracture in the penetrator to having a fractured penetrator will occur somewhere in the vicinity of $\frac{t}{d} \cong 1.0$.

The ability of CTH to predict fracture as described in this report may prove to have more uses than just for predicting fracture of grooved rods during oblique impact with plates of finite thickness. The technique may prove to be transferable to other areas of technology in which ballistic impacts occur in the presence of geometric stress concentrations.

8. References

1. Raftenberg, M. N.; Bjerke, T. W. *Bending of Threaded and Unthreaded Tungsten Rods Under Oblique Impact*; ARL-TR-3578; U.S. Army Research Laboratory: Aberdeen Proving Ground, MD, August 2005.
2. Bjerke, T. W. U.S. Army Research Laboratory, Aberdeen Proving Ground, MD. Private communication, September 2005.
3. Cubit 10.1 User Documentation. http://cubit.sandia.gov/help-version10.1/CUBIT_10.1_User_Documentation.pdf (accessed June 2006).
4. McGlaun, J. M.; Thompson, S. L. CTH: A Three-Dimensional Shock Wave Physics Code. *International Journal of Impact Engineering* **1990**, *10*, 351–360.
5. Meyer, H. W.; Kleponis, D. S. *An Analysis of Parameters for the Johnson-Cook Strength Model for 2-in-Thick Rolled Homogeneous Armor*; ARL-TR-2528; U.S. Army Research Laboratory: Aberdeen Proving Ground, MD, June 2001.
6. Crawford, D. A. Sandia National Laboratories, Albuquerque, NM. Private communication, 20 October 2005.
7. Bell, R. L.; Baer, M. R.; Brannon, R. M.; Crawford, D. A.; Elrick, M. G.; Hertel, E. S., Jr.; Schmitt, R. G.; Silling, S. A.; Taylor, P. A. *CTH User's Manual and Input Instructions, Version 7.0*; Sandia National Laboratories: Albuquerque, NM, April 2005.

NO. OF COPIES	ORGANIZATION
1 (PDF ONLY)	DEFENSE TECHNICAL INFORMATION CTR DTIC OCA 8725 JOHN J KINGMAN RD STE 0944 FORT BELVOIR VA 22060-6218
1	US ARMY RSRCH DEV & ENGRG CMD SYSTEMS OF SYSTEMS INTEGRATION AMSRD SS T 6000 6TH ST STE 100 FORT BELVOIR VA 22060-5608
1	DIRECTOR US ARMY RESEARCH LAB IMNE ALC IMS 2800 POWDER MILL RD ADELPHI MD 20783-1197
3	DIRECTOR US ARMY RESEARCH LAB AMSRD ARL CI OK TL 2800 POWDER MILL RD ADELPHI MD 20783-1197
	ABERDEEN PROVING GROUND
1	DIR USARL AMSRD ARL CI OK TP (BLDG 4600)

NO. OF COPIES	ORGANIZATION
1	TRADOC SYS MANAGER ATZK TS W MEINSHAUSEN FORT KNOX KY 40121-5000
3	COMMANDER US ARMY AMCOM AMSRD AMR PS WF G JOHNSON D KIELSMEIER M BROOKS REDSTONE ARSENAL AL 35898-5247
1	COMMANDER US ARMY AMCOM AMSRD AMR SS K WILLIAMS REDSTONE ARSENAL AL 35898-5247
1	US ARMY ARDEC AMSRD AAR AEM S MUSALLI BLDG 65 S PICATINNY ARSENAL NJ 07806-5000
1	US ARMY ARDEC AMSRD AAR EMB R CARR BLDG 1 PICATINNY ARSENAL NJ 07806-5000
2	US ARMY ARDEC AMSRD AAR AEM M PALATHINGAL M LUCIANO BLDG 65 S PICATINNY ARSENAL NJ 07806-5000
1	US ARMY ARDEC AMSRD AAR AEM L T VELLA PICATINNY ARSENAL NJ 07806-5000
2	US ARMY ARDEC AMSRD AAR AIS SA R CASALE J WALSH PICATINNY ARSENAL NJ 07806-5000
1	US ARMY ARDEC AMSRD AAR AEM L E LOGSDON BLDG 65 PICATINNY ARSENAL NJ 07806-5000
3	US ARMY ARDEC PROJECT MANAGER MANEUVER ARMAMENT SYS SFAE AMO MAS LC R DARCY D RIGOGLIOSO K TARCZA BLDG 354 M829E3 IPT PICATINNY ARSENAL NJ 07806-5000
3	US ARMY ARDEC AMSRD AAR AEE W R FONG J KRAFT S TANG BLDG 3022 PICATINNY ARSENAL NJ 07806-5000
3	COMMANDER US ARMY NGIC LANG SCC W GSTATTENBAUER J MORGAN C AICHES 2055 BOULDERS RD CHARLOTTESVILLE VA 22901-5391
3	INST FOR ADVNCED TCHNLGY THE UNIV OF TEXAS AT AUSTIN S BLESS D BARNETTE B PEDERSON 3925 W BRAKER LN AUSTIN TX 78759-5316
2	SOUTHWEST RESEARCH INST C ANDERSON J WALKER PO DRAWER 28510 SAN ANTONIO TX 78228-0510
1	UNIV OF DAYTON RSCH INST A PIEKUTOWSI 300 COLLEGE PARK DAYTON OH 45469-0182
	ABERDEEN PROVING GROUND
1	DIR USAMSAA AMSRD AMS D APG MD 21005

NO. OF COPIES	ORGANIZATION
38	DIR USARL AMSRD ARL WM EG E SCHMIDT AMSRD ARL WM MB W DEROSSET AMSRD ARL WM TA M BURKINS T HAVEL T JONES M KEELE D KLEPONIS J RUNYEON S SCHOENFELD AMSRD ARL WM TB P BAKER R SKAGGS R BANTON AMSRD ARL WM TC R ANDERSON (2 CPS) J BARB G BOYCE N BRUCHEY R COATES A COPLAND D DIEHL T FARRAND E KENNEDY M FERMAN-COKER K KIMSEY L MAGNESS R MUDD R PHILLABAUM D SCHEFFLER S SCHRAML B SCHUSTER B SORENSEN R SUMMERS W WALTERS C WILLIAMS AMSRD ARL WM TD T BJERKE M RAFTENBERG E RAPACKI S SEGLETES

INTENTIONALLY LEFT BLANK.